

DETECTION OF ATMOSPHERIC CHERENKOV RADIATION USING SOLAR HELIOSTAT MIRRORS

R.A. Ong¹, D. Bhattacharya², C.E. Covault¹,
D.D. Dixon², D.T. Gregorich³, D.S. Hanna⁴, S. Oser¹,
J. Québert⁵, D.A. Smith⁵, O.T. Tümer², and A.D. Zych²

¹*The Enrico Fermi Institute, The University of Chicago,
Chicago, IL 60637, USA*

²*Institute of Geophysics and Planetary Physics, The University of
California, Riverside, CA 92521, USA*

³*IPAC, California Institute of Technology, Pasadena, CA 91125 and
Dept. of Physics and Astronomy, California State University LA,
Los Angeles, CA 90032, USA*

⁴*Department of Physics, McGill University
Montreal, Quebec H3A 2T8, CANADA*

⁵*C.E.N. de Bordeaux-Gradignan, Le Haut Vigneau,
Gradignan 33175, FRANCE*

(To be published in *Astroparticle Physics*)

Abstract

There is considerable interest world-wide in developing large area atmospheric Cherenkov detectors for ground-based gamma-ray astronomy. This interest stems, in large part, from the fact that the gamma-ray energy region between 20 and 250 GeV is unexplored by any experiment. Atmospheric Cherenkov detectors offer a possible way to explore this region, but large photon collection areas are needed to achieve low energy thresholds. We are developing an experiment using the heliostat mirrors of a solar power plant as the primary collecting element. As part of this development, we built a detector using four heliostat mirrors, a secondary Fresnel lens, and a fast photon detection system. In November 1994, we used this detector to record atmospheric Cherenkov radiation produced by cosmic ray particles showering in the atmosphere. The detected rate of cosmic ray events was consistent with an energy threshold near 1 TeV. The data presented here represent the first detection of atmospheric Cherenkov radiation using solar heliostats viewed from a central tower.

1 Introduction

The instruments on the Compton Gamma Ray Observatory (CGRO) have revealed that the gamma-ray sky is rich and exciting. Over 100 point sources of gamma-rays have been detected by the EGRET detector on the CGRO at energies up to 20 GeV [1]. Gamma-rays are detected from objects such as bursts, pulsars (e.g. Crab and Vela), active galactic nuclei (e.g. 3C279, Mrk 421), and nearby galaxies (e.g. LMC), but the majority of the sources are still unidentified with known objects. Largely due to its limited collection area, the EGRET instrument lacks sufficient sensitivity to detect sources above 20 GeV.

Ground-based telescopes have detected TeV gamma-rays from a handful of objects (e.g. Crab, Mrk 421). The detections clearly demonstrate that gamma-ray astronomy can be done from the ground using the atmospheric Cherenkov technique [2]. However, the current generation of atmospheric Cherenkov

telescopes is limited by signal-to-noise considerations to operate at energies above 250 GeV. Therefore, an important goal in gamma-ray astronomy is the exploration of the energy region between 20 and 250 GeV. This region is one of the last remaining windows of the electromagnetic spectrum where no observations have been made. We would like to search this window for possible new astrophysical phenomena, and would like to connect observations made at low energies by satellite experiments (such as EGRET) with ones made at high energies by ground-based observatories. These are the most important scientific motivations for the development of gamma-ray telescopes in this energy regime [3].

1.1 Atmospheric Cherenkov Technique

Although the Earth's atmosphere is opaque to gamma-radiation, the products of extensive air showers created by gamma-rays can be detected at ground level. High energy gamma-rays interact in the upper atmosphere and produce electromagnetic cascades consisting largely of electrons, positrons, and photons. The relativistic electrons and positrons emit Cherenkov radiation which is beamed to the ground. The Cherenkov photons hit the ground with a narrow spread in arrival times (< 40 nsec) and form a circular light pool approximately 250 m across. Atmospheric Cherenkov telescopes, using mirrors and fast photomultiplier tubes (PMTs), detect these photons to reconstruct the energy and direction of the primary gamma-ray. The atmospheric Cherenkov technique has been successfully used for gamma-ray astronomy at energies from 250 GeV to 10 TeV by several observatories, such as Whipple (U.S.), Cangaroo (Australia), and Thémis (France).

Although there are a large number of Cherenkov photons reaching the ground in an air shower, the photons are spread out over a large area, leading to small densities at any given ground location. For example, a shower created by a vertically incident 50 GeV gamma-ray contains, on average, more than 200,000 photons at ground level. However, the mean density within 150 m of the shower axis is only ~ 2.6 photons/m². Small density values require large mirror collection areas in order to concentrate enough Cherenkov light onto the detecting elements of a telescope.

The energy threshold of a Cherenkov telescope is set by its ability to trigger on a signal of Cherenkov photons amidst the background of night sky photons. If we assume that the energy threshold, E_{th} , depends on the minimum signal-to-noise ratio required for triggering, we can derive the approximate way in which the threshold depends on the telescope parameters:

$$E_{\text{th}} \propto \sqrt{B\Omega t / A\epsilon} . \quad (1)$$

Here B is the flux of night sky photons, Ω is the solid angle viewed by the detecting element, t is the trigger time window. A is the telescope mirror area, and ϵ is the efficiency of light collection [4]. We can reduce the energy threshold of a Cherenkov telescope by minimizing the background light level, the field-of-view, and the trigger time window. or by maximizing the photon collection efficiency and the mirror area. There are practical limitations on reducing the field-of-view or time window that are imposed by the physics of the shower. A minimum field-of-view of 0.5° (full angle) is required to contain most of the Cherenkov image. The time window cannot be reduced much below a few nsec, which is the characteristic width of the Cherenkov pulse. The most straight-forward way to lower the energy threshold is to increase the amount of mirror collection area.

Ground-based telescopes using the air shower technique must contend with a large background of showers initiated by isotropic cosmic rays. This background flux is typically two to three orders of magnitude larger than gamma-ray fluxes. In order to reliably detect high energy gamma-rays, Cherenkov telescopes must reject a significant fraction of the cosmic ray showers. At primary energies below 100 GeV, substantial rejection comes from the fact that cosmic ray showers contain much less Cherenkov light than showers initiated by gamma-rays. In cosmic ray showers, a large fraction of the total energy goes into products (hadrons, muons, neutrinos) which do not produce Cherenkov radiation, whereas in gamma-ray showers, all the energy goes into the electromagnetic cascade.

A second observation is that showers produced by cosmic rays are much more chaotic and irregular in development than those initiated by gamma-rays. These development characteristics translate into significant differences between gamma-ray and cosmic ray showers in the angular and lateral distributions of the Cherenkov light. Atmospheric Cherenkov detectors that exploit these shower features are able to reject a substantial fraction of the cosmic ray showers. For example, the Whipple Observatory has used

an imaging technique to reject over 99% of the cosmic ray background. This technique led to the first convincing ground-based detection of gamma-rays [5].

1.2 Large Area Cherenkov Detectors

Current state-of-the-art atmospheric Cherenkov telescopes have mirror areas $\sim 100 \text{ m}^2$, and energy thresholds of $\sim 250 \text{ GeV}$. These experiments sample only a small fraction of the available Cherenkov light. Recently, designs for a number of new large area Cherenkov detectors have been suggested. One design concept (VHEGRA) makes use of large (10 m diameter) reflectors in which each reflector has its own PMT camera [6]. Another group (Telescope Array) is developing a telescope consisting of more than one hundred small (3 m diameter) reflectors [7]. In this design, each reflector would have a camera of sixteen multi-anode PMTs. A third design concept consists of one (or more) large hemispherical reflectors or “bowls” constructed by filling the insides of a cavity in the ground with mirrors [8]. In the most ambitious version of this design, the cavity would be 300 to 400 m across, and a large camera, suspended at the mirror focal point, would follow astronomical sources by rotating to view different parts of the sky.

In each of the design concepts mentioned above, the price of the reflectors themselves dominates the overall cost of the experiment. We are developing an atmospheric Cherenkov detector that makes use of the large mirror area available at central tower solar plants. The great advantage here is that the mirrors have already been built and are available.

1.3 Solar Array Cherenkov Detectors

The idea to use large solar arrays for collecting Cherenkov radiation from air showers was introduced more than a decade ago with application to the solar reflector (heliostat) field of the National Solar Tower Test Facility (NSTTF) at Sandia National Laboratories (Albuquerque NM, USA) [9]. The original design concept was to reflect Cherenkov light from heliostats onto a camera of PMTs located on top of the central tower, viewing the heliostat field. This design had a number of technical problems: 1) the large ($> 1 \text{ m}$ diameter) Cherenkov image sizes produced by the heliostats required very large PMTs, 2) each PMT saw light from more than one heliostat, and 3) designing a detector trigger was difficult because the time of propagation for light from a heliostat to the tower varied, depending on the position of the heliostat and on the inclination angle of the shower.

In 1990, members of our group proposed a gamma-ray observatory using the large heliostat array of the Solar Two Power Plant (Daggett CA, USA) [10, 11]. The proposal suggested the use of an optical secondary located on the central tower. Here, the secondary (either a large mirror or Fresnel lens) serves two important tasks. First, it acts to focus the light from each heliostat down to a small spot that can be collected by a conventional (1-2") PMT. Second, it creates an image of the heliostat field in the focal plane of the secondary. Each heliostat is imaged to a unique location in the image plane. In this way, each PMT sees the light from only one heliostat. The use of secondary optics therefore solves the first two problems associated with the original design concept [9]. The problem of varying time delays remains, but the use of secondary optics allows each PMT to have its own unique delay circuit.

To form an overall experiment trigger, the PMT signals from the heliostats would be selectively delayed and combined. Two possible delay schemes can be imagined. The first scheme would delay the PMT analog signals by means of good quality coaxial cables. The variation in delay lengths would be achieved by programmable switches, and a trigger would be formed from the analog sum of the signals. The second scheme would discriminate the PMT signals at low levels. The digitally delayed discriminator outputs would be combined to form an overall trigger.

In addition to lowering the energy threshold, the use of an array of mirrors also permits measurement of the lateral distribution of the Cherenkov light. As discussed earlier, this distribution can be used to provide separation between showers initiated by gamma-ray and cosmic ray (hadronic) primaries. We are currently examining the degree of separation that could be achieved from a hypothetical large area Cherenkov array using Monte Carlo simulations.

Since 1993, considerable interest has arisen in the possibility of atmospheric Cherenkov telescopes built around solar heliostat arrays. There are now two groups developing prototype experiments based on this design concept. Some of us (JQ and DAS) are involved with a French group initiating an experiment to use up to 180 heliostats of the Thémis solar power plant near Targassonne in the eastern Pyrénées [12].

The remainder are developing a prototype experiment to use either the Solar Two Power Plant or the National Solar Tower Test Facility. To understand the feasibility of the design concept, we have carried out a program of tests at the Solar Two site. The results from this program, which started in April 1994, are the subject of this paper.

1.4 Solar Two Power Plant

The Solar Two Power Plant was constructed from 1979 to 1992, and is located 20 km east of Barstow CA, USA (34.9 N, 116.3 W, 593 m above sea level). Solar Two consists of 1818 heliostats spread out around a central tower, covering an area of approximately 200,000 m². Each heliostat has its own altitude-azimuth drive and local circuitry for tracking control. A heliostat mirror is composed of twelve facets with a total reflective surface of 40 m². The heliostats can be controlled from computers at a central location, or via a specialized interface using a lap-top personal computer.

After a test and evaluation phase, the plant was used for power production until 1988. Recently, a consortium of private and government sponsors formed to refurbish the plant and to resume solar energy production. The refurbishment of the plant started at the end of 1994, and was completed in November 1995. Among other improvements carried out, each heliostat was inspected, (if necessary) repaired, and brought into good optical alignment. The refurbishment of the plant has therefore had an important beneficial impact on its potential as an astronomical site. The Solar Two facility will resume operations for solar power in early 1996 as part of a several-year program.

2 Site Testing Program

We now describe the technical progress that has been made on our design concept. In April 1994, we started a testing program at the Solar Two site. The initial goals of this program were to: 1) characterize the properties of the heliostats, 2) determine the suitability of the site for astronomical purposes, and 3) demonstrate that Cherenkov radiation can be reliably detected above background using solar heliostats. We accomplished each of these initial goals during tests carried out in 1994.

2.1 Heliostat and Site Characterization

In April and August 1994, we spent ten days at the Solar Two site studying the performance of the heliostats and making measurements of the night sky brightness. The results from these studies have been presented elsewhere [13], and therefore, are only briefly discussed here:

1. The tracking and pointing accuracies of the heliostats were measured directly using a laser. The heliostats track smoothly to an accuracy of better than 0.05°.
2. The optical properties of several heliostats were determined by reflecting sunlight onto a target at the top of the central tower. After suitable alignment of the individual mirror facets, the heliostat spot sizes at the tower were measured to be less than 3.0 meters in diameter. Since the angular size of the Sun ($\sim 0.5^\circ$) is comparable to the angular extent of the Cherenkov light in a shower, the measured spot sizes determine the optimal diameter of the secondary.
3. Direct photometric measurements of the night sky brightness due to local light pollution were made from the triggering rate of a collimated PMT. Although light pollution near the horizon was high, the brightness looking down into the heliostat field (where the secondary optics would point) was within 50% of that found at a dark location such as Dugway, Utah, site of the Chicago Air Shower Array (CASA) and Fly's Eye experiments.

The results from these studies encouraged us to build a detector to see atmospheric Cherenkov radiation.

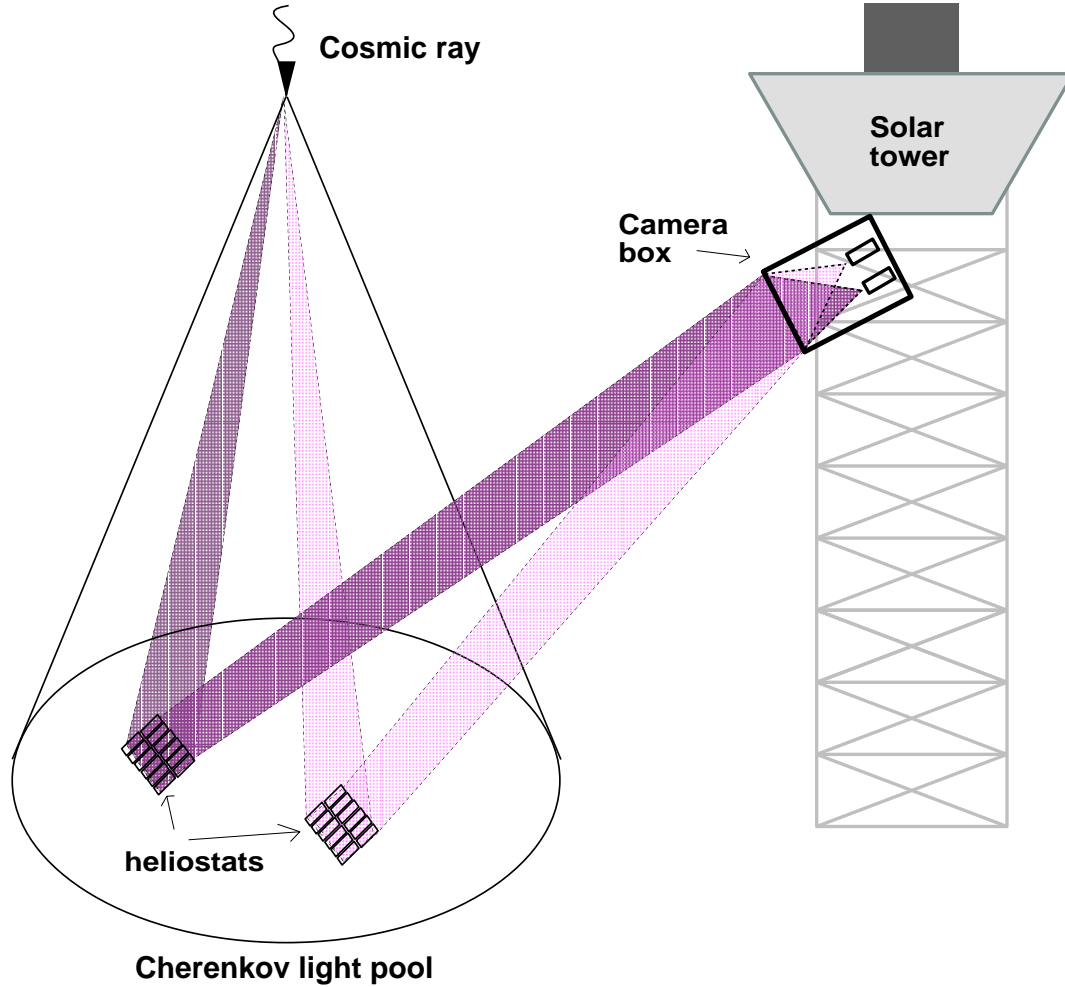


Figure 1: Schematic representation of the detector. A high energy cosmic ray creates an extensive air shower in the atmosphere. The Cherenkov radiation in the air shower is beamed to the ground where it is reflected by heliostats to a camera on the central tower. The camera (located 70 m above ground level) consists of a large Fresnel lens and an array of photomultiplier tubes. The camera box is not drawn to scale.

3 Atmospheric Cherenkov Radiation Detection

3.1 Detector

A schematic representation of the detector is shown in Fig. 1. High energy cosmic rays interact in the upper atmosphere (~ 10 km altitude) to create extensive air showers. The Cherenkov light in the shower propagates to ground level. The primary optic consisted of four solar heliostats with a total reflective area of 160 m^2 . The heliostats reflected Cherenkov radiation to a camera box on the central tower. The camera consisted of a secondary optic (Fresnel lens) and photomultiplier tubes (PMTs). The PMT signals were electronically recorded by a data acquisition (DAQ) system.

3.1.1 Heliostat Selection

We selected four heliostats [14] in the northeast quadrant of the Solar Two heliostat field, as shown in Fig. 2. The heliostats were approximately halfway out into the field and were chosen to lie along a circular arc so that each heliostat was at the same approximate distance from the tower. In this way, there were no relative differences in the light propagation times from the heliostats to the tower for vertically incident

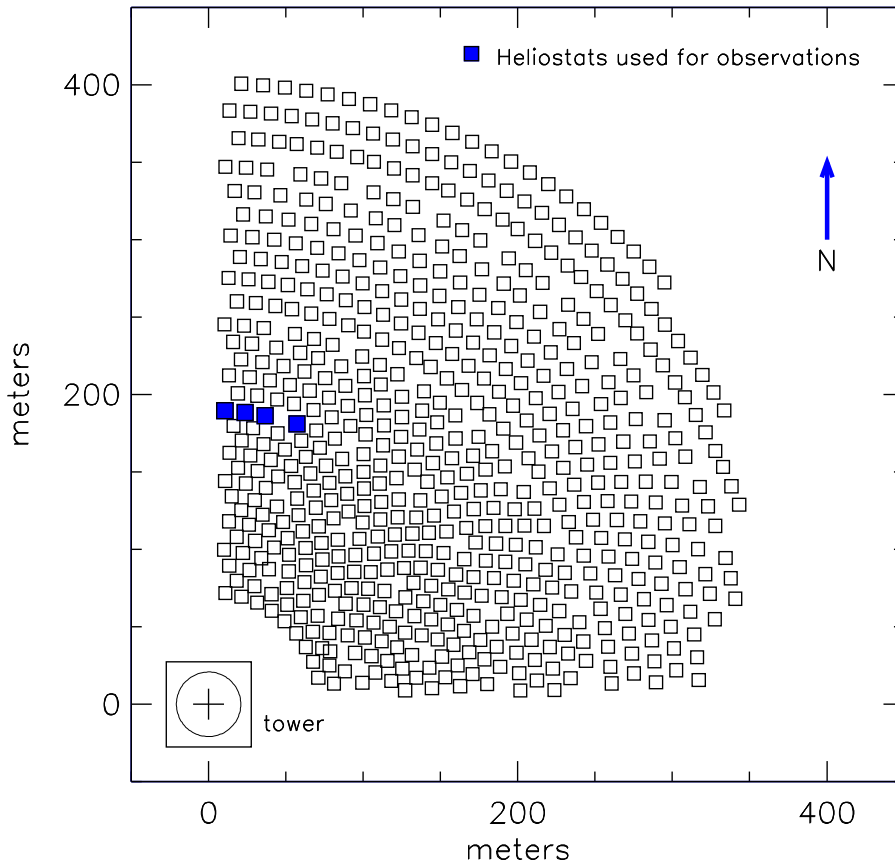


Figure 2: Northeast quadrant of the Solar Two heliostat field. Each square represents a heliostat consisting of a 40 m^2 mirror and an altitude-azimuth drive. The four heliostats used in this work are indicated by the shaded squares.

showers. The mirror facets of the selected heliostats were washed and aligned using the image of the Sun on a large target on the tower. The azimuth and elevation headings of the heliostats were controlled using a custom-made interface module [15] and a lap-top personal computer.

3.1.2 Camera

The camera box was made from an aluminum frame of dimensions $32'' \times 42'' \times 84''$. Aluminum panels painted black covered the frame to make a light-tight enclosure. A shutter attachment was mounted at one end of the box (along the major axis). This attachment held a $31'' \times 41'' \times 3/16''$ Fresnel lens (Edmund Scientific G31,139) and a removable wooden shutter. The lens had a focal length of $40''$ and a typical transmission of 85% for wavelengths between 400 and 1000 nm. Four fast 2" photomultiplier tubes (Hamamatsu R2154-UV) were mounted at the focal plane of the Fresnel lens so that the images of four heliostats were focused onto the PMTs (one heliostat per PMT). The PMTs were operated with the cathode at negative high voltage (typically -1.05 kV), and with a typical current amplification of $\sim 5 \times 10^5$. The high voltage was provided by a 32-channel programmable supply (LeCroy 4032).

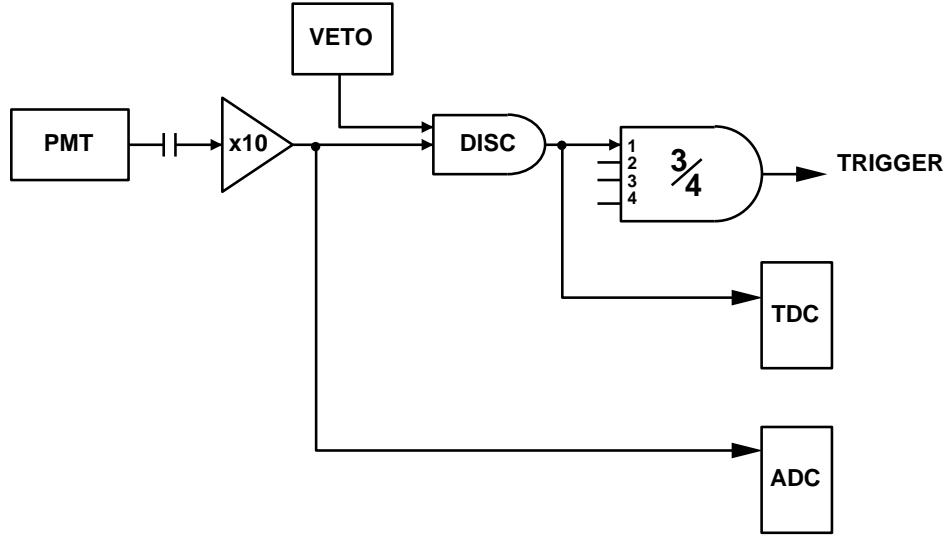


Figure 3: Functional diagram of the electronics used (one of four channels). The photomultiplier tube (PMT) signal is amplified (x10) and discriminated. The discriminated signal is routed into the trigger logic. A trigger is formed when any three out of four PMTs are above threshold within a window of 40 nsec. The PMT time-of-arrival is recorded in a time-to-digital converter (TDC), and its pulse-height is recorded in an analog-to-digital converter (ADC). A veto circuit is used to eliminate pulses of long duration created by light from artificial sources.

3.1.3 Electronics

A schematic diagram of the electronic circuitry is shown in Fig. 3. The electronics consisted of commercial modules using the NIM and CAMAC standards. The PMT signals were carried to the electronics via 15 m of coaxial cable (RG-58A/U). The signals were AC-coupled through amplifiers (LeCroy 612AM) with a signal gain of ten. We used amplifiers in order to keep the PMT gains below 10^6 . The amplified signals were delayed by 70 m of coaxial cable (RG-8/U), and their charges were measured by analog-to-digital converters (ADCs). The ADCs (LeCroy 2249W) had 11-bit resolution, a conversion scale of 0.25 pC/count, and were gated by a 40 nsec wide pulse.

The amplified signals were also discriminated (LeCroy 623B) at discriminator levels between 90 mV and 225 mV. The discriminated outputs were used to form a trigger coincidence, and to stop time-to-digital converters (TDCs). The TDCs (LeCroy 2228A) had a dynamic range of 11-bits with a least count value of 250 psec. The trigger logic (LeCroy 365) required the overlap of at least three (out of four) 40 ns wide pulses. The trigger rates for three and four-fold coincidences, as well as the PMT single counting rates, were recorded by scalars (LeCroy 2551).

An important part of the electronic circuitry was a veto circuit designed to eliminate the effects of background light produced by man-made sources. The most significant sources of this type were aircraft warning beacons at a neighboring power plant (located 3 km southwest of the Solar Two site). These beacons produced flashes of light which were intense, but which occurred at a low repetition rate (~ 1 Hz). The PMT pulses caused by the flashes were much longer in duration than Cherenkov signals (100 μ sec versus 10 nsec). Therefore, a veto circuit based on pulse length could be used to inhibit the trigger logic during noise pulses. The veto circuit was made by splitting the amplified signal from each PMT into two paths. Along one path, the signal was delayed through 30 m of coaxial cable (RG-58A/U). Along the other path, an updating discriminator (Phillips 711) was used to indicate the presence of a signal that remained over threshold for more than 100 nsec. In this manner, all spurious long pulses were eliminated from the trigger.

3.1.4 Data Acquisition

The trigger signal generated a gate for the ADCs and a common start for the TDCs. The data recorded in the ADCs and TDCs were digitized and read out through a 16-bit parallel CAMAC interface (Kinetic Systems 3922) to an Intel 286-based personal computer. The data were acquired on a local hard disk and then transferred via modem to a remote Unix workstation.

3.2 Operating Conditions

The data used in this work were taken on two moonless nights (November 4 and 5, 1994). On the first night, the weather conditions were good, with clear skies and a wind speed less than 20 mph at ground level. On the second night, there was a significant amount of high level haze. Before the tests started, we studied the pointing of each heliostat by locating the image of the Sun on the tower. We recalibrated the absolute heliostat pointing for each night of operation.

At the start of nighttime operation, high voltage was applied to the PMTs, but the camera shutter was kept closed. The PMT single counting rates and three-fold and four-fold coincidence rates were measured for a range of different discriminator settings. We repeated these measurements with the camera shutter open, but with the heliostats oriented randomly in the sky (i.e. with the heliostats not pointed to a common location). Finally, the heliostats were aligned to a common point in the sky. The trigger rates and pulse-height distributions were recorded for various discriminator settings and for various heliostat zenith angle configurations.

3.3 Results

3.3.1 Trigger Rates

The PMT single counting rates were estimated from scaler counters that monitored each PMT. The three and four-fold coincidence rates were calculated from additional scaler counters or from the TDC information. The two methods used to estimate the coincidence rates gave identical results. In addition, the distributions of the time intervals between successive events predicted coincidence rates that were consistent with the measured rates. For example, Fig. 4 shows the time interval distribution of successive events for data taken on November 4. The shape of the distribution for small time differences indicates that the detector deadtime was small ($< 5\%$).

Table 1 shows typical PMT single counting rates and three and four-fold coincidence rates for the detector under various operating conditions. The coincidence rates demonstrate that the detector was triggering on atmospheric Cherenkov radiation since coincidences only occurred when the heliostats were aligned to a common point in the sky. The fact that the coincidence window was short (40 nsec) excluded the possibility that artificial light sources caused accidental coincidences. The pulses of individual PMT signals in coincidence events were examined on a storage oscilloscope, and were found to have very sharp rise-times (~ 3 nsec) and profiles consistent with Cherenkov radiation produced in the atmosphere.

Table 1 also shows that when a single heliostat was pointed away from the common point in the sky, the four-fold coincidence rate went to zero. This demonstrates that each PMT saw light from only one heliostat and that there was no significant cross-talk from one heliostat to another.

Fig. 5 shows the three and four-fold coincidence rates as a function of the PMT discriminator threshold for data taken on two different nights (Night 1: November 4, Night 2: November 5, 1994). The rates decrease monotonically with increasing discriminator level, showing that the detector energy threshold rose as the discriminator level was increased. The three-fold coincidence rate was a factor of two larger than the four-fold rate, indicating a significantly lower energy threshold for the three-fold events. The coincidence rates observed on the first night were higher than those observed on the second night for the same operating conditions. This change was presumably caused by a reduction in the clarity of the atmosphere during the latter observations.

Assuming that the detector was triggering on atmospheric Cherenkov radiation produced by cosmic ray interactions in the atmosphere, we expect an approximate reduction in the trigger rate of 3.2 for each factor of two increase in threshold ($E^{-1.66}$ integral spectrum). For the observations made on the first night, we measured reduction factors of 3.0 and 2.9 for the three and four-fold coincidence data, respectively. On

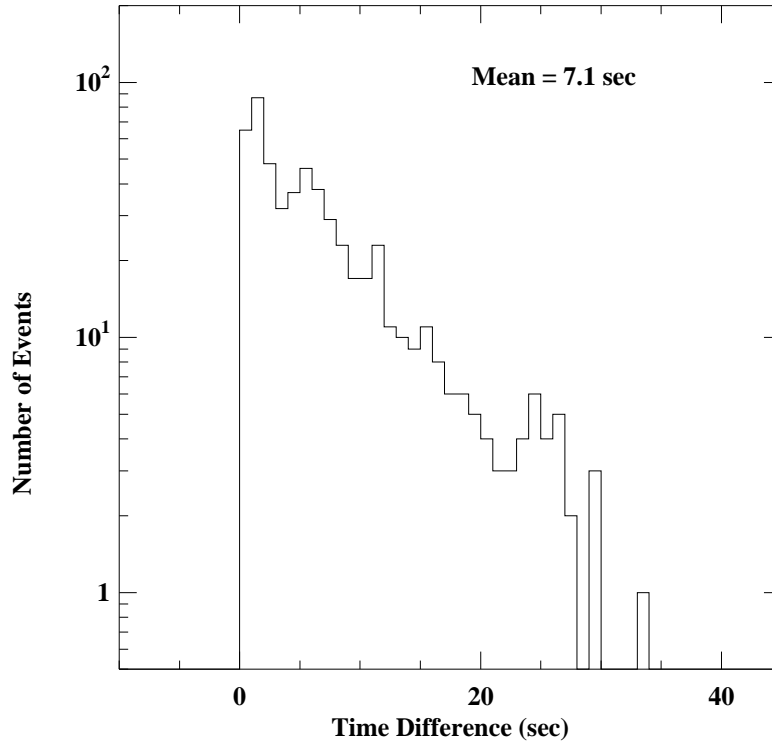


Figure 4: Distribution of time intervals between successive events. Data shown were taken with the detector triggering on vertical air showers on November 4, 1994, at a PMT threshold of 125 mV. The data are well described by a single exponential function with mean (7.1 ± 0.5) sec. The mean agrees with the observed event rate of 9.1/minute.

Table 1: Typical PMT single counting rates and trigger coincidence values (in 10 minute intervals) for various detector configurations at a PMT threshold of 125 mV. The detector configurations were: A) high voltage on and shutter closed, B) high voltage on, shutter open, and heliostats not aligned, C) high voltage on, shutter open, and three heliostats aligned, D) high voltage on, shutter open, and four heliostats aligned. The range in the single counting rates reflects gain differences among the PMTs. The difference in the single counting rates between configurations B and C reflects the fact that the heliostats were pointed to different sky locations in these two configurations. For configurations C and D, the heliostats were aligned to detect vertical air showers. The three-fold coincidence values include those events which are also four-fold.

Configuration	PMT single count. rate	3-fold coin.	4-fold coin.
A	3.6-5.5 Hz	None	None
B	4.5-6.8 kHz	None	None
C	4.8-7.2 kHz	75	None
D	4.8-7.2 kHz	91	48

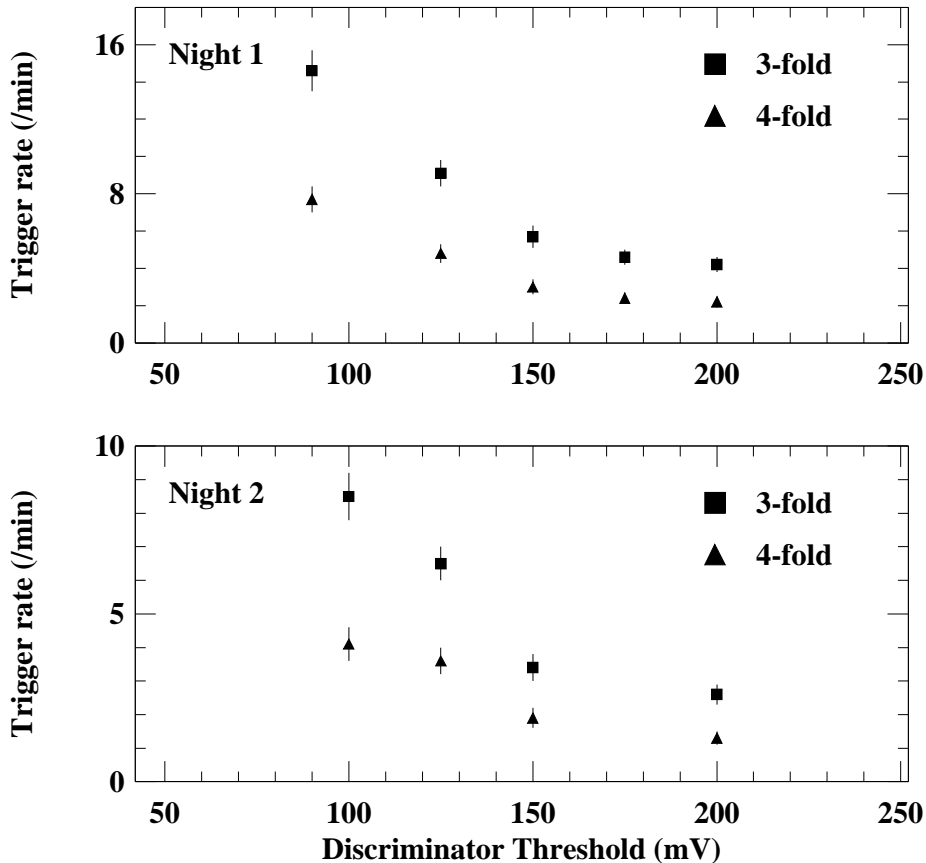


Figure 5: Detector three and four-fold coincidence rates as a function of PMT discriminator threshold. The data for observations made on two different nights are shown for the detector triggering on vertical air showers (Night 1: November 4, 1994, Night 2: November 5, 1994). The atmospheric visibility on the second night was degraded by the presence of a layer of high haze.

the second night, we measured factors of 3.3 and 3.2, respectively. The measured reduction factors (with a typical uncertainty of 10%) are in good agreement with expectations, supporting the assumption that the detector was triggering on air showers induced by cosmic rays.

Fig. 6 shows the variation in the trigger rate as a function of the air shower zenith angle. We saw a significant dispersion in the trigger rates at zenith angles greater than 20° ; the values shown in Fig. 6 are typical ones. The trigger rate decreased monotonically with increasing zenith angle, which is consistent with the expected increase in energy threshold due to increased atmospheric depth.

3.3.2 Pulse-Height Measurements

The raw pulse-height distributions measured for one of the four PMTs are shown in Fig. 7. These data come from a ninety minute period on Night 2 at a discriminator threshold of 125 mV. The mean PMT pulse-height in four-fold coincidence events was larger than that in three-fold events, as expected.

Fig. 7 also shows the pulse-height distributions for the same PMT when it did not trigger the discriminator in a three-fold coincidence event (Fig. 7c), and when random gate pulses were applied to the ADC

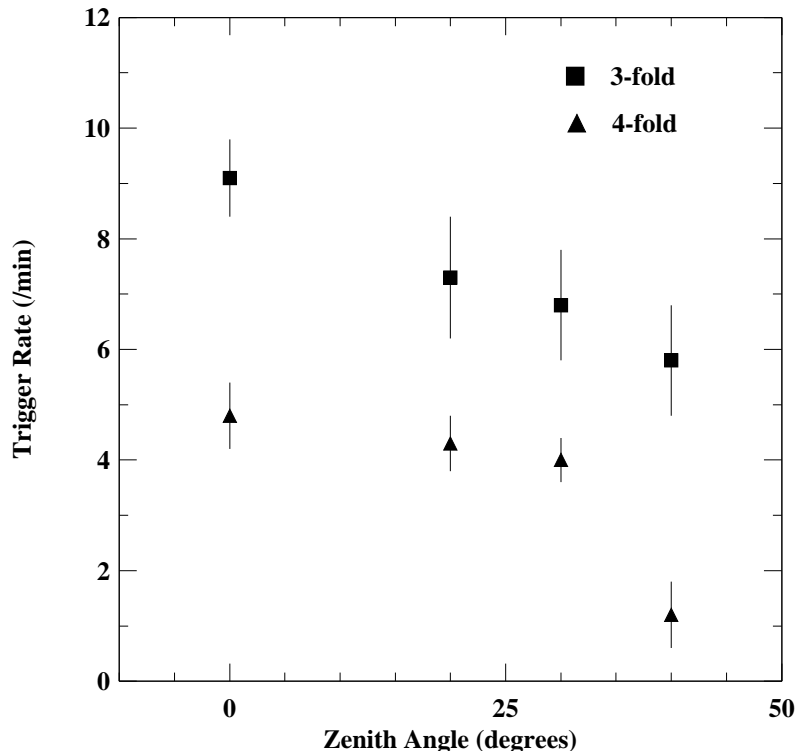


Figure 6: Detector three and four-fold coincidence rates as a function of air shower zenith angle. The data were taken on November 4, 1994 at a discriminator threshold of 125 mV.

(Fig. 7d). The mean pulse height for signals below the discriminator threshold is much less than the mean for signals above threshold. The mean in the former case is not zero, however, because in such events the PMT detected Cherenkov signals, but at levels below threshold. The mean pulse-height for the ADC gated randomly is close to zero, which is consistent with the expected value of the ADC pedestal.

There is significant overlap between the distributions of 7b and 7c, which shows that some pulses which participate in the trigger contain less charge than pulses which are below trigger threshold. We attribute this effect to the different pulse shapes produced in the showers. Some are of low (voltage) amplitude but are longer than pulses with equal charge but higher amplitude. This lack of a constant pulse shape means that a voltage threshold is not seen as a sharp edge in charge plots such as those shown in Fig. 7.

The mean pulse-height as a function of discriminator threshold is shown in Fig. 8 for each PMT in the detector. Although there is some variation in gain from one PMT to another, the average pulse-heights monotonically increase with increasing threshold, as expected.

3.3.3 Energy Threshold

In the previous section, we have demonstrated that the coincidence rates and pulse-height distributions are in agreement with expectations. The data clearly show that the detector was triggering on cosmic ray air showers. Here we verify that the pulse-height data are consistent with what we expect from cosmic ray showers triggering the detector at the observed coincidence rate. To verify the consistency of the data, we calculate the median energy for cosmic rays triggering the detector by two different techniques. First, we compare the measured coincidence rates to the known integral cosmic ray flux, and second, we use a

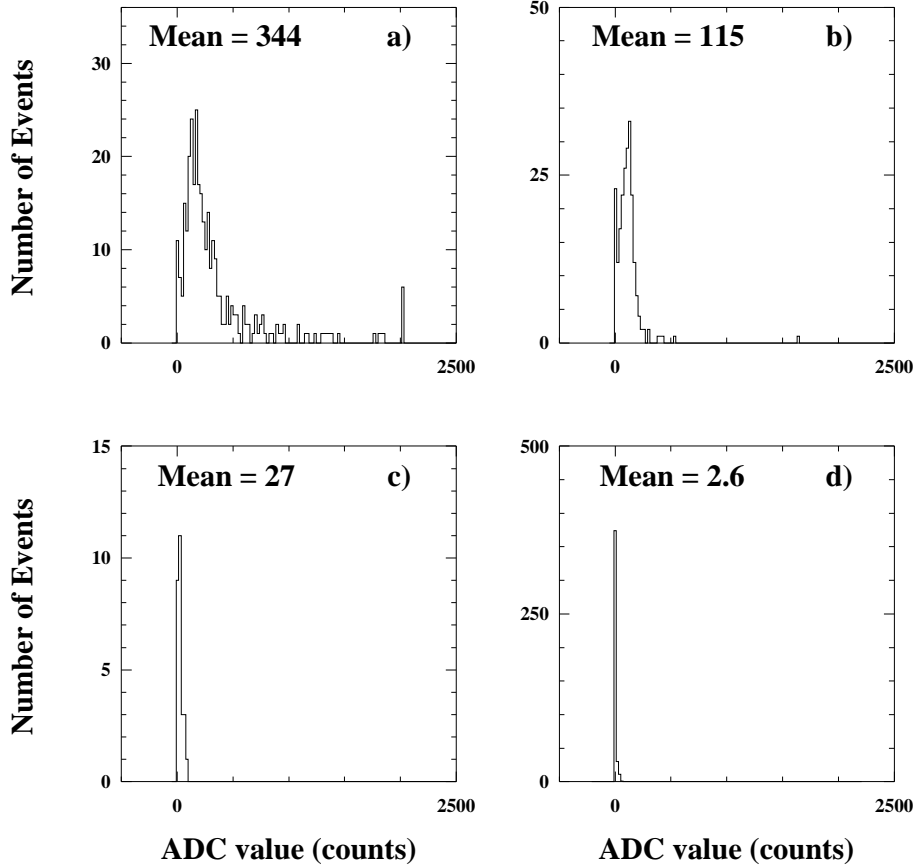


Figure 7: Pulse height distributions for one of the four PMTs (PMT 2). Histograms of the ADC count values are shown for: a) four-fold coincidence events, b) three-fold coincidence events where the PMT participated in the trigger, c) three-fold coincidence events where the PMT did not participate in the trigger, and d) events in which the ADC was gated by a random trigger pulse. The three-fold coincidence data shown in b) does not include those events which were also four-fold coincident. The data come from a ninety minute period on November 5, 1994, with the detector triggering on vertical air showers at a discriminator threshold of 125 mV.

simulation to reproduce the median observed pulse-height. For these calculations, we use vertical air shower data taken over a period of sixty minutes on Night 1, at a discriminator threshold of 125 mV.

The mean three-fold coincidence rate for these data was 9.1/minute; the mean four-fold rate was 4.8/minute. In order to estimate the median cosmic ray energy of the detector, we need to determine the expected coincidence rate as a function of cosmic ray energy. We estimate the integral cosmic ray flux, $\Phi(> E)$, the effective collection area, A , and the field-of-view of the detector, Ω . The expected coincidence rate, R , is then:

$$R = \Phi(> E) \cdot A \cdot \Omega . \quad (2)$$

Our estimate of the integral cosmic ray flux is based on direct measurements made by balloon and satellite experiments [16]. We convert the differential spectra of the direct measurements into an integral flux by

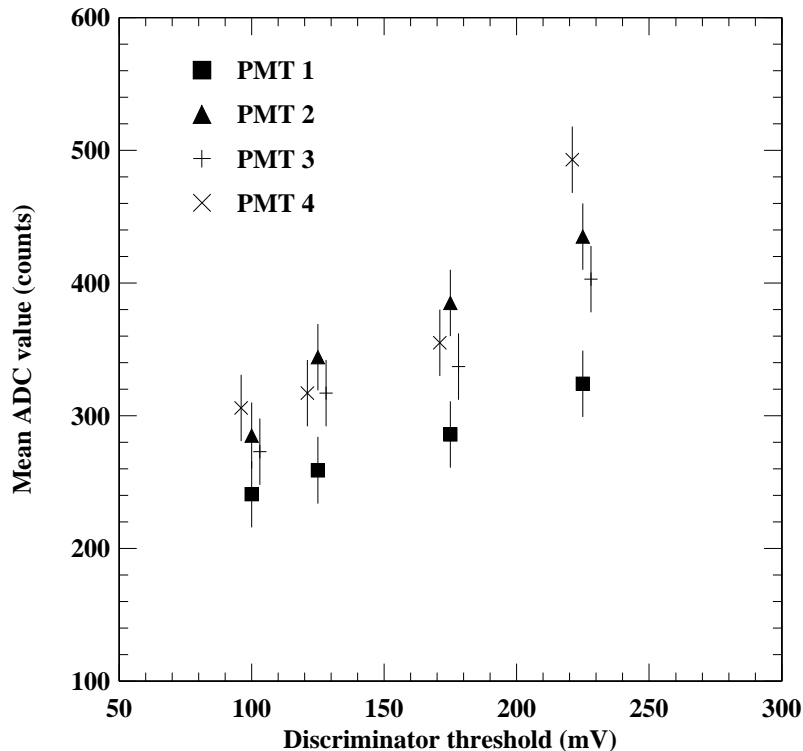


Figure 8: Mean pulse-heights for each PMT as a function of discriminator threshold for four-fold coincidence events. The data come from a ninety minute period on November 5, 1994, with the detector triggering on vertical air showers.

Table 2: Integral flux estimates for various cosmic ray nuclei. The flux above 1 TeV is expressed in the form $\Phi(E > 1 \text{ TeV}) = \Phi_0 \cdot E^{-\alpha}$, where E is the energy in TeV. The fourth column lists the fractional percentage of each species at 1 TeV.

Species	Φ_0 ($/\text{cm}^2/\text{sr}/\text{sec}$)	α	Fraction (%)
H	5.87×10^{-6}	1.72	35
He	4.14×10^{-6}	1.68	25
CNO	2.67×10^{-6}	1.62	16
NeS	1.91×10^{-6}	1.61	11
Fe	2.13×10^{-6}	1.60	13

estimating the power law dependence of the spectra at 1 TeV. We correct for the fact that the direct techniques measure cosmic ray energies in units of energy/nucleon whereas air shower detectors trigger on the total energy. Table 2 shows our estimates for the integral fluxes above 1 TeV for the five major species of cosmic ray nuclei.

From Table 2, the total integral cosmic ray flux above 1 TeV is estimated to be $(1.67 \pm 0.22) \times 10^{-5}$ particles/ $\text{cm}^2/\text{sec}/\text{sr}$. This flux represents the number of particles hitting the upper atmosphere of the

Earth per unit time per unit solid angle. Our experiment, however, triggers on the air shower produced from the cosmic ray interaction. We must therefore account for the variation in shower size for different cosmic ray nuclei. Heavy nuclei interact sooner in the atmosphere and deposit a larger fraction of their energy into the hadronic cascade than do light nuclei. These effects lead to a significant decrease in the Cherenkov light yield for air showers produced by nuclei of increasing mass.

We estimate the amount of Cherenkov light expected for different cosmic ray nuclei by means of the Monte Carlo simulation MOCCA [17]. For the hadronic and electromagnetic cascades that develop from the primary interaction, the trajectories of all particles with energies above 200 keV are followed until they reach the ground or are absorbed. The Cherenkov photons produced in the shower are propagated to the ground, taking into account the wavelength-dependent absorption of the atmosphere from Mie and Rayleigh scattering. We determine the mean Cherenkov photon density at ground level from those photons that are within a radius of 100 m of the shower axis and that arrive within 40 nsec of the shower front. The same average density in showers initiated by 1 TeV protons is found in helium showers at approximately 1.5 TeV, nitrogen showers at 2.4 TeV, sulfur showers at 3.0 TeV, and iron showers at 3.3 TeV. We derive a corrected estimate for the integral cosmic ray flux above 1 TeV of $(9.1 \pm 1.4) \times 10^{-6}$ particles/cm²/sec/sr, where the flux has been corrected for composition effects (i.e. it describes the total flux of particles that would yield showers having the same Cherenkov photon density as that in a shower produced by a 1 TeV proton).

We estimate the field-of-view for the detector to be $(7.9 \pm 0.5) \times 10^{-5}$ sr, and the collection area to be $(3.1 \pm 0.8) \times 10^8$ cm². The field-of-view is determined from a calculation which convolutes the measured heliostat beam size with the dimensions of the camera box aperture. The collection area is determined from the simulation. The error in the collection area results largely from our uncertainty in the value of the energy threshold and the fact that the collection area depends on threshold. We use Eq. (2) to determine a median energy for the detector for proton showers of 1.24 ± 0.19 TeV for the three-fold coincidence data, and 1.79 ± 0.25 TeV for the four-fold coincidence data. This determination assumes an overall cosmic ray integral spectral index of 1.66.

We also determine the median detection energy from the pulse-height distributions derived from the same data set. Assuming that the observed Cherenkov photon density on the ground is proportional to the primary particle energy, the detected number of photoelectrons for each tube, N_{pe} , can be represented as:

$$N_{pe} = y_p E \epsilon A, \quad (3)$$

where y_p is the expected Cherenkov photon density on the ground per unit of proton energy, E is the energy, ϵ is the efficiency of photon detection, and A is the projected area of each heliostat. Using the simulation, we estimate that $y_p \sim 56$ photons/m²/TeV near 1 TeV and that $\epsilon = (7.3 \pm 1.5) \times 10^{-3}$. The value for ϵ includes the wavelength-dependent reflectivity of the heliostat mirror (0.51), the fraction of the heliostat image within the aperture of the Fresnel lens (0.14), the transmission of the Fresnel lens (0.85), the fraction of the Fresnel image collected by the PMT (0.80), and the quantum efficiency of the PMT (0.15). The projected area of the heliostat is 32.7 m² for these data.

The scale conversion between the number of photoelectrons incident at the PMT face and the measured pulse-height (in ADC counts) was determined by measuring the pulse-height distribution of a PMT from the camera viewing a 0.6 m x 0.6 m x 0.64 cm piece of acrylic scintillator. The photoelectron yield of the scintillator was measured as part of a different experiment [18]. This procedure yielded a conversion factor of 9.1 ± 1.1 ADC counts/photoelectron. Using this factor, the median pulse-height was 14.9 ± 1.8 photoelectrons for the three-fold coincidence data, and 21.3 ± 2.6 photoelectrons for the four-fold coincidence data. Using Eq. (3), we can therefore estimate a median energy of the detector for proton showers of 1.12 ± 0.23 TeV for the three-fold coincidence data, and 1.60 ± 0.32 TeV for the four-fold coincidence data. The errors in the energy estimations are dominated by our uncertainty in the value of ϵ . Table 3 shows the median energy estimations by the two different methods. Within the uncertainties, the two methods agree.

The lowest energy threshold obtained for the detector was on the first night of operation at a discriminator threshold of 90 mV. In this configuration, the three-fold coincidence rate was 14.6/minute. From these data, we estimate a median detection energy for proton showers of 940 ± 130 GeV. Since 500 GeV gamma-rays produce showers with a comparable amount of Cherenkov radiation to showers initiated by 1 TeV protons, the median energy for the detector described in this paper was near or below 500 GeV for gamma-ray showers.

Table 3: Median proton energies for the three and four-fold coincidence data by the two different methods described in the text.

Method	E (3-fold)	E (4-fold)
Rate	1.24 ± 0.19 TeV	1.79 ± 0.25 TeV
Pulse-height	1.12 ± 0.23 TeV	1.60 ± 0.32 TeV

In addition, during the tests, we made no attempt to explore how low in energy threshold the detector would reliably operate. Since signal-to-noise was not a problem in our tests, the detector could clearly have operated at lower energies. Such operation was not attempted experimentally due to lack of time. We can estimate the minimum energy threshold from the observed PMT single counting rates and from laboratory measurements using the same type of PMT [19]. Assuming a maximum accidental trigger rate of 10 Hz, we estimate a minimum single PMT threshold of approximately six photoelectrons. This PMT threshold translates into an overall energy threshold of ~ 450 GeV for vertically incident proton showers using this initial prototype detector.

4 Conclusions

We have built a prototype atmospheric Cherenkov detector using solar heliostat mirrors as the primary reflecting element. The detector was operated successfully in November, 1994. The observed detection rate of cosmic ray air showers was consistent with our expectations, and with a median proton energy of 1 TeV. We are now developing a first-generation experiment that will employ up to fifty heliostats and several large area secondary collectors. This experiment could take initial data in 1997.

Acknowledgements

We would like to acknowledge the cooperation and help of Southern California Edison in the tests at the Solar Two Power Plant. We thank Charles Lopez, Roy Takekawa, and Robert Edgar, and gratefully acknowledge the help of Mark Chantell and Anthony Miceli. This work was supported by the National Science Foundation, the Institute of Particle Physics of Canada, and the California Space Institute. RAO wishes to acknowledge the support of the W.W. Grainger Foundation and the Alfred P. Sloan Foundation.

References

- [1] D.J. Thompson et al., *Ap. J. Suppl.* **101** (1995) 259.
- [2] For a recent review of ground-based gamma-ray astronomy, see R.C. Lamb, R.A. Ong, C.E. Covault, and D.A. Smith, *Proc. of the 1994 Snowmass Summer Study, Particle and Nuclear Astrophysics and Cosmology in the Next Millennium*, ed. by E.W. Kolb and R.D. Peccei (World Scientific, Singapore, 1995) 295.
- [3] See, for example, T.K. Gaisser et al., *Opportunities in Cosmic-Ray Physics and Astrophysics*, (National Academy Press, Wash. D.C., 1995) 3.
- [4] Trevor C. Weekes, *Phys. Reports* **160** (1988) 1.
- [5] G. Vacanti et al., *Ap. J.* **337** (1991) 467.
- [6] C.W. Akerlof, *Nucl. Inst. and Meth.* **A264** (1988) 74 and *Very High Energy Gamma Ray Array (VHEGRA)*, proposal submitted to the Smithsonian Astrophysical Observatory (unpublished, 1995).

- [7] M. Teshima et al., *Proc. of the International Workshop Towards a Major Atmospheric Cherenkov Detector*, ed. by P. Fleury and G. Vacanti (Editions Frontieres, Paris, 1992), 255.
- [8] S.P. Ahlen et al., *Nucl. Inst. and Meth.* **A351** (1994) 493.
- [9] S. Danaher et al., *Solar Energy* **28** (1982) 355.
- [10] The plant was originally known as the Solar One Pilot Power Plant. Its name was changed in 1993 to the Solar Two Power Plant as part of a refurbishment and upgrade.
- [11] O.T. Tümer et al., *Nucl Phys. B (Proc. Suppl.)* **14A** (1990) 351.
- [12] E. Paré, *Proc. of the International Workshop Towards a Major Atmospheric Detector Cherenkov Detector II*, ed. by R.C. Lamb (Iowa State Univ., 1993) 250.
- [13] R.A. Ong et al., *Proc. of the International Workshop Towards a Major Atmospheric Cherenkov Detector III*, ed. by T. Kifune (Universal Academy Press, Tokyo, 1994) 295.
- [14] The identification numbers of the heliostats used were 1401, 1403, 1405, and 1407. Their locations were (10.6,189.6) m, (23.7,188.4) m, (36.7,186.3) m, and (57.1,181.1) m, respectively, in a coordinate system with (x) pointing east and (y) pointing north.
- [15] Stimulator interface made by Advanced Thermal Systems, Denver CO, USA.
- [16] S. Swordy, *Proc. of the 23rd International Cosmic Ray Conf. (Calgary)*, ed. by D.A. Leahy, R.B. Hicks, and D. Venkatesan (World Scientific, Singapore, 1994) Rapporteur Volume 243.
- [17] A.M. Hillas, *Proc. of the 19th International Cosmic Ray Conf. (La Jolla)*, ed. by F.C. Jones, J. Adams, and G.M. Mason (Scientific and Technical Information Branch (NASA), Washington D.C., 1985) 3 (1985) 445.
- [18] A. Borione et al., *Nucl. Inst. and Meth.*, **A346** (1994) 329.
- [19] In the laboratory, we used a constant intensity light source to illuminate a PMT. We adjusted the source intensity so that the single PMT counting rate matched the observed detector rate at the same PMT discriminator threshold used in the detector. We then measured the dependence of the PMT counting rate versus discriminator threshold.